Mitochondrial Oscillations and Waves in Cardiac Myocytes: Insights from Computational Models

Ling Yang,[†§] Paavo Korge,[‡] James N. Weiss,[†‡] and Zhilin Qu[†*]
[†]Department of Medicine (Cardiology) and [‡]Department of Physiology, David Geffen School of Medicine at University of California, Los Angeles, California; and [§]Center for Systems Biology, Suzhou University, Jiangsu, China

ABSTRACT Periodic cellwide depolarizations of mitochondrial membrane potential (Ψ_M) which are triggered by reactive oxygen species (ROS) and propagated by ROS-induced ROS release (RIRR) have been postulated to contribute to cardiac arrhythmogenesis and injury during ischemia/reperfusion. Two different modes of RIRR have been described: Ψ_M oscillations involving ROS-sensitive mitochondrial inner membrane anion channels (IMAC), and slow depolarization waves related to mitochondrial permeability transition pore (MPTP) opening. In this study, we developed a computational model of mitochondria exhibiting both IMAC-mediated RIRR and MPTP-mediated RIRR, diffusively coupled in a spatially extended network, to study the spatiotemporal dynamics of RIRR on Ψ_M. Our major findings are: 1), as the rate of ROS production increases, mitochondria can exhibit either oscillatory dynamics facilitated by IMAC opening, or bistable dynamics facilitated by MPTP opening; 2), in a diffusively-coupled mitochondrial network, the oscillatory dynamics of IMAC-mediated RIRR results in rapidly propagating (~25 μm/s) cellwide Ψ_M oscillations, whereas the bistable dynamics of MPTP-mediated RIRR results in slow (0.1–2 μm/s) Ψ_M depolarization waves; and 3), the slow velocity of the MPTP-mediated depolarization wave is related to competition between ROS scavenging systems and ROS diffusion. Our observations provide mechanistic insights into the spatiotemporal dynamics underlying RIRR-induced Ψ_M oscillations and waves observed experimentally in cardiac myocytes.

INTRODUCTION

As the dominant source of ATP generation in cardiac myocytes, mitochondria are essential for normal cardiac function (1,2). An adult cardiac myocyte contains ~7000 mitochondria, which are positioned along the myofibrils in a highly ordered network. Under normal conditions, mitochondria are polarized, with a membrane potential (Ψ_M) of ~−180 mV maintained across the inner membrane by the respiratory chain. Ψ_M provides the driving force for proton influx through ATP synthase, which is coupled to ATP synthesis. When mitochondria depolarize ($\Psi_M \sim 0$), however, ATP synthase reverses, consuming ATP to pump protons out of the matrix. It is well known that excessive levels of reactive oxygen species (ROS) can trigger Ψ_M depolarization. Fluorescence indicators used to measure Ψ_M, such as tetramethylrhodamine ethyl ester or tetramethylrhodamine methyl ester, generate ROS when illuminated by laser light, conveniently allowing the effects of ROS production on Ψ_M to be directly investigated (3). Using two-photon confocal excitation to illuminate a small area in a tetramethylrhodamine ethyl ester-loaded cardiac myocyte, Aon et al. (4,5) showed that locally generated ROS triggered cellwide Ψ_M oscillations and fast propagating waves, with a wave velocity estimated at 22 μm/s. Using similar methods, Brady et al. (6) also showed cellwide Ψ_M fluctuations and traveling waves; however, the wave velocity was <0.1 μm/s. In our own experiments using whole-cell illumination instead of localized photoactivation, we have observed both Ψ_M oscillations and slow waves, the latter wave velocities ranging from 0.1 to 2.2 μm/s (7) (and H. Honda, J. –H. Yang, and J. N. Weiss, unpublished data). Theories have been proposed to explain the underlying mechanisms of Ψ_M oscillations and waves, such as percolation theory (5,8), coupled oscillators (9), and excitable medium (7,10,11). However, a cohesive understanding of the spatiotemporal dynamics underlying these observations is lacking.

Mechanistically, evidence has been presented that cellwide Ψ_M oscillations and waves are caused by a positive feedback loop in ROS-induced ROS release (RIRR) (3–6, 11–14). Under normal conditions, mitochondrial respiration is accompanied by low-level ROS production neutralized by powerful antioxidant systems. During metabolic stresses (e.g., ischemia and reperfusion), however, ROS levels can increase, which in turn can trigger additional ROS production and release from the mitochondria. Two different mechanisms of RIRR have been proposed: one is related to the inner membrane anion channel (IMAC) regulation (4,5,12), and the other to the mitochondrial permeability transition pore (MPTP) regulation (3,6,11,13,14).

Aon et al. (4) proposed IMAC-mediated RIRR to explain cellwide oscillations and waves observed in their experiments, from which Cortassa et al. (12) developed a mathematical model incorporating the sensitivity of IMAC to superoxide anion (O^-_2) in the intermembrane space into their previous model of mitochondrial energetics (15). That is, as matrix O^-_2 generated by electron transport complexes diffuses into the intermembrane space, IMAC open probability increases, creating a positive feedback loop releasing

Submitted March 30, 2009, and accepted for publication December 15, 2009.

*Correspondence: zqu@mednet.ucla.edu

Editor: Michael D. Stern.

0006-3495/10/04/1428/11 $2.00

doi: 10.1016/j.bpj.2009.12.4300

more O^-_2 into the intermembrane space. This positive feedback loop can cause limit cycle oscillations, providing a mechanistic explanation for the Ψ_M oscillations observed in their experiments. Brady et al. (6), on the other hand, found that the slow mitochondrial waves in their experiments were associated with matrix calcein release indicating MPTP opening, and were also inhibited by MPTP blockers such as cyclosporin A. They postulated that Ψ_M oscillations were mediated by MPTP-induced RIRR. No model has yet been presented for MPTP-mediated RIRR.

So far, no spatial model of either IMAC-mediated or MPTP-mediated RIRR has been developed to investigate how the mitochondrial network responds to these dynamical behaviors. Even if different RIRR mechanisms are involved, an interesting question is why the wave velocities are so different (two orders of magnitude), despite the same method of induction by laser illumination.

In this study, we first developed a single mitochondrion model of RIRR that includes both IMAC-mediated and MPTP-mediated RIRR. We then diffusively coupled individual mitochondria in a two-dimensional array of voxels, each containing the single mitochondrion model with appropriate matrix, intermembrane space, and cytoplasmic volumes. We show that, depending on the rate of ROS production, the single mitochondrion model can exhibit either limit-cycle Ψ_M oscillations due to the IMAC-mediated RIRR or bistability due to the MPTP-mediated RIRR. In the two-dimensional mitochondrial network, localized elevation of ROS production (analogous to localized laser-triggered ROS production) induces global Ψ_M oscillations due to rapid propagation of IMAC-mediated RIRR, whereas MPTP-mediated RIRR causes slow Ψ_M waves, consistent with both sets of experimental observations. We show that the self-amplifying nature of these RIRR processes results in a natural progression from cellwide Ψ_M oscillations to irreversible Ψ_M depolarization.

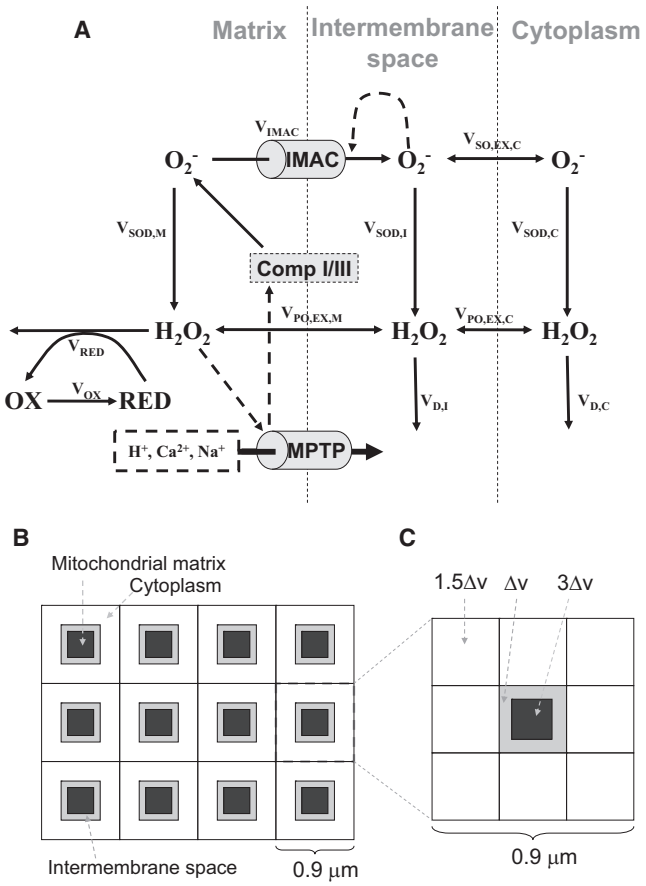

FIGURE 1 Schematic diagrams of ROS-induced ROS release models. (*A*) The single mitochondrion model including both IMAC- and MPTP-mediated pathways. (*B*) Schematic diagram of the spatial model of mitochondrial network. (*C*) For computational purposes, each unit is composed of 3×3 voxels representing a mitochondrion with its surrounding cytoplasm: the center voxel represents both the matrix (*black*) and the intermembrane space (*gray*), and the surrounding eight lattices are the neighboring cytoplasm. The relative volumes of each type of voxel are marked proportionately to the basic unit of volume Δv, corresponding to a volume ratio among matrix, intermembrane space, and cytoplasm of 3:1:12.

MATHEMATICAL MODELS

Single mitochondrion model incorporating both IMAC-mediated and MPTP-mediated RIRR

We developed a single mitochondrion model that incorporates both IMAC-mediated and MPTP-mediated RIRR (Fig. 1 *A*). Three compartments, the mitochondrial matrix, intermembrane space, and cytoplasm, are included. O^-_2 is produced in the matrix by Complexes I and III (16–19), and can only exit from the matrix into the intermembrane space through IMAC. (We ignored the minor component of O^-_2, which directly exits Complex III to the intermembrane space, as it had no qualitative effect on dynamics.) In the matrix, intermembrane space, and cytoplasm, O^-_2 is converted by superoxide dismutase (SOD) to H_2O_2 at rates $V_{SOD,M}$, $V_{SOD,I}$, and $V_{SOD,C}$, respectively. H_2O_2 is allowed to diffuse freely between all three compartments, and in the matrix is degraded by peroxidases such as glutathione peroxidase, which in the process converts reducing cofactors (RED, such as GSH) to their oxidized forms (OX, such as GSSG) at a rate V_{RED}. In the cytoplasm and intermembrane space, H_2O_2 is degraded directly (e.g., by catalase and peroxidases) at rates $V_{D,I}$ and $V_{D,C}$, respectively. For simplicity, we omitted the RED/OX system in the intermembrane and cytoplasmic spaces, because it had no qualitative effects on dynamics.

We modeled IMAC-mediated RIRR following Cortassa et al. (12). When O^-_2 production in the matrix increases to a critical level, its leakage through IMAC into the intermembrane space further activates IMAC, which releases more O^-_2 from the matrix, forming a positive feedback loop. As IMAC opening is progressively activated, Ψ_M becomes depolarized. However, as O^-_2 released into the

intermembrane space and cytoplasm is converted by SOD to H_2O_2, IMAC deactivates, which allows electron transport to restore Ψ_M. This mechanism is consistent with the experimental finding that SOD mimetics prevented Ψ_M depolarization due to IMAC-mediated RIRR (4), but not MPTP-mediated RIRR (6,13).

We introduced MPTP-mediated RIRR into the model as follows. As proposed by Brady et al. (6,11), we assume that when H_2O_2 generated from O^-_2 accumulates sufficiently, a downstream product of H_2O_2, such as hydroxyl radicals or an oxidized lipid, activates MPTP opening. Because the specific downstream peroxide or oxidized lipid has not been identified, for simplicity we assume it to be proportional to H_2O_2 concentration. MPTP-mediated RIRR is then modeled as follows. When matrix H_2O_2 accumulates sufficiently (associated with RED depletion), MPTP opens, depolarizing Ψ_M. Consistent with experimental findings (20,21), we assume that when MPTP opening occurs, O^-_2 production by Complexes I/III transiently accelerates. This leads to more H_2O_2 production, which further activates MPTP in a positive feedback loop.

Our model has several differences from the model of Cortassa et al. (12). In our model, O^-_2 generation is an adjustable parameter, rather than a variable linked to energy metabolism, so that it can be flexibly manipulated to study dynamics. In addition, our model includes a formulation of MPTP regulation, which was not modeled by Cortassa et al. The differential equations and details of the mathematical models are presented in the Appendix.

Two-dimensional mitochondrial network model

We simulated a two-dimensional mitochondrial network consisting of 50 × 10 coupled voxels (Fig. 1 *B*), with each unit containing the three-compartment single mitochondria model described above. The spatial scale of a unit is 0.9 μm, and thus two-dimensional network size is 45 × 9 μm, representing ~1/3 of a typical myocyte's area. Both O^-_2 and H_2O_2 diffuse freely between the intermembrane space and adjacent cytoplasmic space, as well as in the cytoplasmic space. To diffusively couple the network, we divided each unit into 3 × 3 voxels (Fig. 1 *C*), with the center voxel representing the volumes of matrix and the intermembrane space, and the surrounding eight voxels the volume of surrounding cytoplasm. The matrix, intermembrane, and cytoplasm compartments were fixed at a volume ratio of 3:1:12 (mitochondria accounts for ~25% of the cellular space (22)). Note that in Fig. 1 *C*, the voxels are not drawn to scale. Further modeling and computational details are presented in the Appendix.

Numerical methods

The steady state and its stability of the single mitochondrion model were analyzed using MATLAB (The MathWorks, Natick, MA). The differential equations of the single mitochondrion model and the network model were numerically solved by Euler method with a time step 10^{-4} s.

RESULTS

Temporal dynamics of the single mitochondrial model

In the single mitochondrion model, O^-_2 production rate (V_s) was set to $V_S = k_{shunt}(1 + \alpha_{MPTP})$, where k_{shunt} represents O^-_2 production due to endogenous respiration modified by external factors such as laser scanning-induced O^-_2 production, and $k_{shunt}\alpha_{MPTP}$ is the additional component of O^-_2 production associated with MPTP opening. When k_{shunt} is small (normal conditions), O^-_2 and H_2O_2 concentrations are low and the open probabilities of IMAC and MPTP are close to zero, and Ψ_M is accordingly well polarized and stable (Fig. 2). As k_{shunt} increases, however, matrix O^-_2 progressively increases. When k_{shunt} reaches > 0.025 mM/s, the leak of matrix O^-_2 through IMAC into the intermembrane space raises intermembrane space O^-_2 sufficiently to cause regenerative IMAC opening due to the positive feedback, releasing more O^-_2 from the matrix. Once O^-_2 released from the matrix is degraded by cytoplasmic SOD, IMAC deactivates, restoring Ψ_M until sufficient O^-_2 builds up in the matrix to begin a new cycle. When k_{shunt} exceeds 0.105 mM/s, however, cytoplasmic SOD cannot effectively degrade cytoplasmic O^-_2 to a low enough level to deactivate IMAC. At this point, the steady state becomes stable again and oscillations cease, with Ψ_M remaining depolarized. The mechanism of limit-cycle oscillations due to IMAC-mediated RIRR is similar to that proposed by Cortassa et al. (12).

With further increases in k_{shunt}, MPTP-mediated RIRR comes into play. At a critical value (0.16 mM/s in Fig. 2, *A* and *B*), matrix O^-_2 elevates H_2O_2 (via SOD) to a level that triggers the MPTP opening, which, in turn, transiently further accelerates O^-_2 production by Complex I/III, forming another positive feedback loop causing bistability. In the bistable regime, the O^-_2 and H_2O_2 concentrations can either reside in a low stable state, with MPTP closed, or a high stable state with MPTP open (Fig. 2 *B*), depending on the initial conditions of the system. As shown in Fig. 2 *D*, when the initial H_2O_2 is low in the intermembrane space, MPTP are at the lower steady state (*dashed line* in Fig. 2 *D*). When the initial H_2O_2 was high, they transition to the higher steady state (*solid line* in Fig. 2 *D*). For $k_{shunt} >$ 0.22 mM/s, both O^-_2 and H_2O_2 increase as k_{shunt} increases and MPTP open completely (Fig. 2, *A* and *B*). Thus, as k_{shunt} gradually increases from a low number (e.g., 0.15 mM/s) to a high number (e.g., 0.25 mM/s), H_2O_2 jumps suddenly (*dashed arrow* in Fig. 2 *B*) to a very high level, and then increases further as k_{shunt} increases due to the transient acceleration of O^-_2 production when MPTP opens. In Fig. 2 *E*, we show the steady states versus k_{shunt} and the RED_{Total}

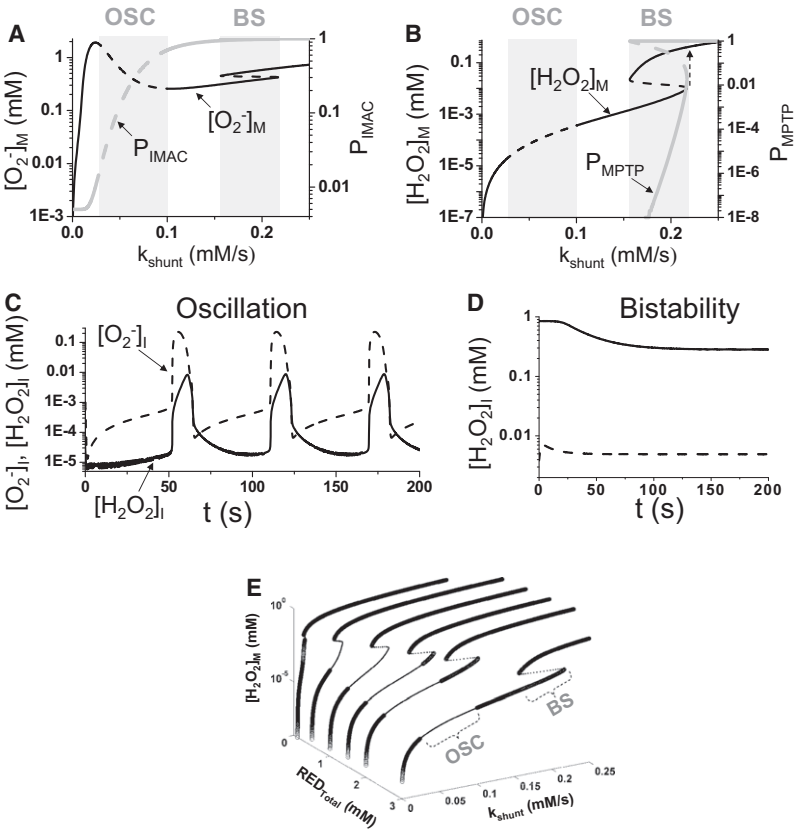

FIGURE 2 Dynamical behaviors of the single mitochondrion model. (*A*) Steady-state matrix superoxide concentration ($[O^-_2]_M$, *black line*) and IMAC open probability (P_{IMAC}, *gray line*) versus k_{shunt}. Dashed segments are unstable steady states. (*B*) Steady-state matrix H_2O_2 concentration ($[H_2O_2]_M$, *gray line*) and MPTP open probability (P_{MPTP}, *gray line*) versus k_{shunt}. Dashed segments are unstable steady states. Loss of stability of the steady state leads to oscillations (OSC zones in *A* and *B*) and bistability (BS zones in *A* and *B*). Dashed arrow indicates that as k_{shunt} increases continuously, a sudden jump occurs in H_2O_2 concentration. (*C*) The intermembrane superoxide concentration ($[O^-_2]_I$, *dashed line*) and intermembrane H_2O_2 concentration ($[H_2O_2]_I$, *solid line*) versus time for k_{shunt} = 0.08 mM/s, which is in the oscillatory regime. (*D*) The intermembrane H_2O_2 concentration in the bistable regime showing two stable steady states (*solid* and *dashed lines*) resulted from two initial conditions at k_{shunt} = 0.2 mM/s. (*E*) Steady-state matrix H_2O_2 concentration ($[H_2O_2]_M$) versus k_{shunt} and RED_{Total}. The thick segments are the stable steady states. The thin segments are unstable steady states. "OSC" and "BS" mark the oscillatory and bistable regions, respectively.

(total GSH/GSSH) in a three-dimensional plot, showing that as RED_{Total} decreases, both the oscillatory and bistable regions shrink and eventually disappear, i.e., MPTP remains open at even very low k_{shunt} values. This illustrates the critical importance of antioxidants.

We also studied how other parameters affect the oscillatory and bistable dynamics. Increasing the maximum O^-_2 release rate (k_{IMAC}) from 0.5 s^{-1} to 5 s^{-1} narrowed the oscillatory regime from the k_{shunt} interval [0.025, 0.1] to [0.025, 0.075], and the period of oscillation decreased from 35 s to 5 s. k_{IMAC} had little effect on bistable behavior due to MPTP opening, however. The Hill coefficient and dissociation constant used in formulating the open probabilities of IMAC and MPTP also affect the ranges of oscillatory and bistable dynamics. For instance, when the Hill coefficient for the IMAC open probability function was reduced from 3 to 2, oscillations occurred over a much narrower k_{shunt} interval, although the MPTP transition was not significantly affected. Similarly, when the MPTP open probability function was reduced from 10 to 2, bistability occurred over a much narrower k_{shunt} interval, although IMAC-mediated RIRR was not significantly affected.

In summary, in this model, IMAC-mediated RIRR causes limit cycle oscillations, whereas MPTP-mediated RIRR results in bistability. As will be demonstrated below, these two dynamics result in different spatiotemporal dynamics in the mitochondrial network.

Spatiotemporal dynamics of the mitochondrial network model

To study how the dynamics of IMAC-mediated and MPTP-mediated RIRR affect the cellwide behavior of the mitochondrial network, we incorporated the single mitochondrion volume units into a two-dimensional array, coupled by diffusion of O^-_2 and H_2O_2 through the cytoplasmic space, as shown in Fig. 1, *B* and *C*. To mimic the localized laser scanning protocol used by Aon et al. (5) to induce IMAC-mediated RIRR, we increased k_{shunt} in a small area of 7 × 7 units (*cyan voxel* in Fig. 3 *C*) in the center of the two-dimensional lattice (Fig. 3 *C*). Due to high k_{shunt} in this area, O^-_2 accumulates to a high enough level to induce limit cycle oscillations as a result of IMAC-mediated RIRR. O^-_2 released from this area diffuses to neighboring regions, elevating intermembrane space O^-_2 sufficiently to induce IMAC opening in adjacent mitochondria. This results in a O^-_2 wave originating from the central area, which propagates outwardly (Fig. 3 *A*), triggering cellwide Ψ_M depolarization (Fig. 3 *B*). Subsequently, as matrix O^-_2 released into the intermembrane and cytoplasmic space is dismutated, IMAC shuts off and Ψ_M repolarizes. This process repeats itself, producing periodic cellwide Ψ_M oscillations (Fig. 3, *C* and *D*). For the parameter settings used in the two-dimensional model, the Ψ_M depolarization wave propagated at a speed of ~25 μm/s, in agreement with experimental

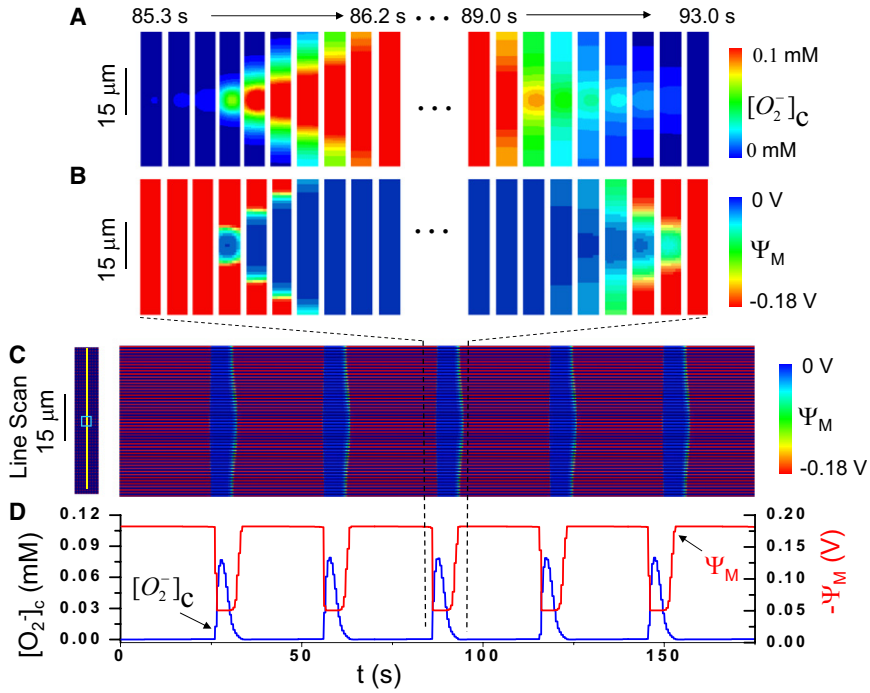

FIGURE 3 Cellwide Ψ_M oscillations due to fast waves of IMAC-mediated RIRR. (*A–C*) Periodic cellwide Ψ_M oscillations over a long timescale are shown in the line scan in panel *C*, with the scanned line and laser stimulated area as marked in the left panel. For one of these cellwide oscillations (between the *dashed lines*), panels *A* and *B* show snapshots of cytoplasmic O^-_2 and Ψ_M at uniform time intervals corresponding to the start (*left panels*) and end (*right panels*) of the oscillation. The mitochondrial depolarization starts from the laser stimulated area (*cyan box* in the *left panel* in *C*) and propagates to both ends of the whole cell. (*D*) The average Ψ_M and O^-_2 of the network versus time. In this simulation, k_{shunt} was set to be 0.2 mM/s in the mitochondria in the center region (*cyan box* in the *left panel* in *C*) and 0.05 mM/s elsewhere.

observations by Aon et al. (5). Since propagation is fast, mitochondria in the whole system appear to oscillate almost synchronously when imaged at frame speeds >1 s, as typical in experiments (Fig. 3, *C* and *D*).

To mimic the whole-cell laser-scanning protocol used by Brady et al. (6) to induce MPTP-mediated RIRR, we increased k_{shunt} to 0.2 mM/s over the whole network, and set four rows of mitochondria at the bottom to an even higher value (0.35 mM/s), to reflect a degree of spatial heterogeneity in the network (i.e., a localized region responding to the same laser intensity with greater O^-_2 production). In this case, a Ψ_M depolarization wave originating from the left end (which is first to exceed the bistability threshold due to the higher k_{shunt} value) propagates slowly through the network, with a wave velocity of 2.1 μm/s. The wave velocity depends strongly on the rate of H_2O_2 degradation or buffering determined by the parameters k_{RED}, $k_{D,I}$, and $k_{D,C}$. As the values of these parameters increases, wave velocity slows due to enhanced H_2O_2 degradation, which is equivalent to reducing the excitability of the medium. For example, when k_{RED} was increased from 3000 s^{-1} to 10,000 s^{-1}, the velocity decreased from 7 μm/s to 2 μm/s (Fig. 4 *B*). This velocity can be further reduced if we also increase the H_2O_2 degradation rate in the intermembrane and cytoplasmic space, biologically corresponding to GSH/GSSH ratios, peroxidase, and catalase activities in these compartments. For example, by adding H_2O_2 degradation to the cytoplasm, we could reduce the wave velocity to 0.3 μm/s.

To simulate the effects of SOD mimetics, we increased $k_{M,SOD}$ from 0.01 mM/s to 1.0 mM/s. For parameters corresponding to IMAC-mediated waves in Fig. 3, the oscillations disappeared. For the parameters corresponding to slow MPTP-mediated waves in Fig. 4, however, the slow waves still occurred. This is consistent with the experimental finding that SOD mimetics prevented Ψ_M depolarization due to IMAC-mediated RIRR (4), but not MPTP-mediated RIRR (6,13).

Finally, we mimicked a scenario in which k_{shunt} increases linearly as a function of time. This would correspond to a situation in which ongoing cycles of IMAC-mediated RIRR cause:

1. Progressive depletion of antioxidant capacity (e.g., the GSH/GSSG ratio decreases); and

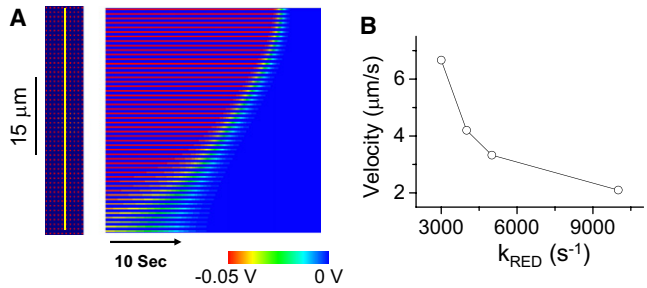

FIGURE 4 MPTP-mediated slow Ψ_M depolarization wave. (*A*) Space-time plot of Ψ_M recorded along the yellow line indicated on the left, after simulated laser stimulation of the whole area. The mitochondrial depolarization wave begins from the bottom and propagates slowly to the top, taking 24 s to propagate 50 μm. (*B*) The wave velocity versus k_{RED}. k_{shunt} was set to 0.35 mM/s in the bottom four rows of mitochondria and 0.2 mM/s elsewhere.

2. Progressive damage to the distal electron transport chain and/or progressive release of matrix cytochrome *c*, such that O^{-}_{2} production from reduced Complexes I/III progressively increases over time (23).

Fig. 5 shows that under these conditions, a series of Ψ_M oscillations due to IMAC-mediated RIRR culminates in sustained IMAC-mediated Ψ_M depolarization, followed later by a slow Ψ_M depolarization wave due to MPTP-mediated RIRR. Eventually, MPTP opening becomes irreversible after the final slow Ψ_M depolarization wave. Although we assumed, for simplicity, a linear increase of k_{shunt} over time, a nonlinear pattern would produce the same qualitative results, altering only the time points at which bifurcations occurred.

DISCUSSION

In this study, we developed a mitochondrial model exhibiting both IMAC-mediated and MPTP-mediated RIRR, and examined how the dynamics of these two RIRR mechanisms interact to produce Ψ_M oscillations and waves in a two-dimensional diffusively coupled mitochondrial network. In the single mitochondrion model, we find that IMAC-mediated RIRR generates limit-cycle dynamics, which in the network produces cellwide Ψ_M oscillations due to fast propagating Ψ_M depolarization waves. In contrast, MPTP-mediated RIRR causes bistable dynamics, which generates slowly propagating waves in the mitochondrial network, eventually leading to irreversible Ψ_M depolarization.

These findings recapitulate experimental observations in isolated myocytes subjected to laser-induced ROS. Consistent with the findings of Aon et al. (4,5) in which laser illumination of a small spot induced cellwide Ψ_M oscillations with a fast wave velocity at ~22 μm/s, IMAC-mediated RIRR reproduces a comparable wave-conduction velocity due to the rapid diffusion of O^{-}_{2} released from the matrix into the intermembrane space. Once released from the matrix, however, O^{-}_{2} degradation in the intermembrane space and cytoplasm is much faster than its production. O^{-}_{2} thus returns quickly to a level which causes IMAC to shut off until O^{-}_{2} accumulates again in the matrix for the next cycle. This is the classical mechanism of positive feedback causing oscillations through substrate depletion (24). The wave is mediated by the diffusion of O^{-}_{2} from one unit to the other to activate IMAC opening, forming a classic excitable medium.

MPTP-mediated RIRR, on the other hand, occurs in the model with an initially higher O^{-}_{2} production rate, consistent with the larger region illuminated by the laser protocol used by Brady et al. (6). The resulting higher matrix O^{-}_{2} production leads (via SOD) to higher matrix H_2O_2 levels and its downstream products, which triggers MPTP opening. MPTP opening transiently accelerates O^{-}_{2} production from Complexes I/III (20,21), generating more H_2O_2 in a positive feedback cycle which results in bistability. The wave velocity for MPTP-mediated RIRR is much slower (0.1–2 μm/s). In excitable media, wave velocity is determined by diffusion rates and excitability, such that faster diffusion or greater excitability gives rise to faster wave velocity. As the diffusion constants of O^{-}_{2} and H_2O_2 were set to be the same in our model, the differences in wave velocity are due to the differences in the excitability between the IMAC-mediated and MPTP-mediated RIRR processes. Fig. 4 *B* demonstrates that the H_2O_2 scavenging rate is a major factor lowering the excitability of MPTP-mediated RIRR, because increasing the H_2O_2 degradation rate reduces the velocity.

Consistent with the experimental findings of Aon et al. (4,5) that MPTP inhibitors such as cyclosporine A did not inhibit IMAC-mediated, cellwide synchronous Ψ_M oscillations, we found that preventing MPTP opening in the model also did not prevent IMAC-mediated Ψ_M oscillations. Similar to the model of Cortassa et al. (12), our model predicts that interventions which reduce O^{-}_{2} production (k_{shunt}) or increase O^{-}_{2} scavenging (k_{RED}) will suppress IMAC-mediated Ψ_M oscillations, as observed experimentally (12). Finally, Aon et al. (25) reported that the susceptibility of permeabilized myocytes to Ψ_M depolarization depended on the GSH/GSSH ratio, with a ratio of 150:1–100:1 favoring the IMAC-mediated Ψ_M depolarization, and a ratio of <50:1 favoring the MPTP-mediated Ψ_M depolarization. In our model, the GSH/GSSG ratio is represented phenomenologically as the RED/OX ratio, which ranged from 9:1 to 1.4:1

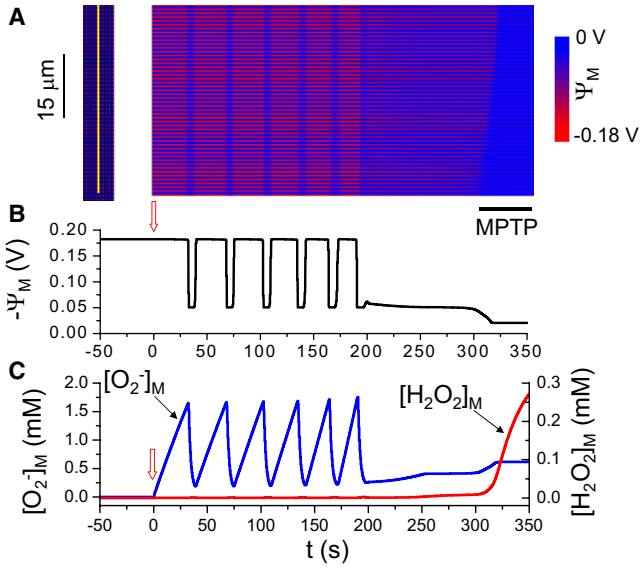

FIGURE 5 IMAC-mediated Ψ_M oscillations triggering an MPTP-mediated final depolarization wave. (*A*) Space-time plot of Ψ_M recorded along the yellow line indicated at the left. O^{-}_{2} production rate increased progressively over time, most rapidly in the lower four rows of mitochondria (where $k_{shunt} = 0.35[0.3 + 0.7 \text{ min } (1,e^{0.02t}/150)]$), and more slowly elsewhere ($k_{shunt} = 0.2[0.3 + 0.7 \text{ min } (1,e^{0.02t}/150)]$). (*B*) Average Ψ_M versus time. (*C*) Mitochondrial O^{-}_{2} (*blue*) and H_2O_2 (*red*) concentrations versus time. k_{shunt} was initially zero and started to increase at the upward arrows. Black bar below the snapshot indicates the final MPTP-mediated slow wave.

during IMAC-mediated Ψ_M oscillations, and <0.03:1 during MPTP-mediated Ψ_M depolarization, in qualitative agreement with these experimental results. Consistent with the findings of Brady et al. (6) that the SOD mimetic TMPyP blocked IMAC-mediated RIRR oscillations without preventing slow waves due to MPTP-mediated RIRR, we reproduced the same results by increasing the SOD activity in our model.

We previously reported that isolated myocytes exposed to anoxia-reoxygenation initially developed both fast reversible Ψ_M oscillations, followed subsequently by a slow Ψ_M depolarization wave (7). Like laser-induced injury, we speculated that the ROS burst upon reoxygenation set into motion progressively increasing ROS production, resulting from ROS-induced damage to electron transport complexes impeding electron flow through the distal respiratory chain. Under these conditions, redox centers in Complex I or III remain partially reduced and generate excessive O^-_2. As this excessive O^-_2 production persists, it consumes antioxidants and further impairs electron transport in adjacent mitochondria (by similarly damaging their electron transport chain), further increasing O^-_2 production until IMAC opening is triggered and IMAC-mediated RIRR propagates rapidly through the cell. During IMAC-mediated cellwide ROS oscillations, progressive ROS toxicity accumulates, further accelerating O^-_2 production and reducing antioxidant capacity until O^-_2 and H_2O_2 levels reach the threshold for MPTP activation, producing a final slow irreversible wave. As shown in Fig. 5, the features of our model, in which separate dynamical mechanisms account for IMAC-mediated and MPTP-mediated Ψ_M waves, predict this behavior when O^-_2 production rate k_{shunt} is progressively increased over time. Because our model assumes that O^-_2 production due to MPTP opening is persistent, Ψ_M remains irreversibly depolarized at the end. However, the burst of O^-_2 production with MPTP opening may only be transient (20,21), due to loss of pyridine nucleotides with prolonged MPTP openings, resulting in oxidation of electron transport redox centers. Depending on the amplitude and duration of the transient O^-_2 burst that occurs with MPTP opening, as well as the value of k_{shunt}, oscillatory behavior can result, such that slow Ψ_M depolarization waves from MPTP-mediated RIRR can be either reversible or irreversible. In addition, in our model, we only allowed the O^-_2 to exit the mitochondria through the IMAC, but it should be noted that O^-_2 can also exit through MPTP once it opens. This limitation does not affect the results shown in Figs. 4 and 5, as IMAC channels are always open before the MPTP opens. However, if MPTP opening is oscillatory, rather than bistable, the interactions between IMAC and MPTP oscillations could be affected by O^-_2 efflux through both channels.

In this study, we used a simplified model to study the oscillatory and wave dynamics of mitochondria depolarization, ignoring the detailed regulation of energy metabolism and other mechanisms of metabolic oscillations as shown in previous modeling studies (15,26–31). We assumed a constant O^-_2 production rate, whereas this rate is variable in real systems. However, because the dynamical bifurcations are set by reaching threshold concentrations of key ROS species, nonlinear O^-_2 production rates should affect the dynamics only quantitatively, and not qualitatively. Another limitation is that many of the details of the proposed regulatory mechanisms assumed in the model remain controversial or incompletely defined (e.g., sensitivity of IMAC channels to intermembrane space O^-_2, the identity of the precise ROS species activating MPTP opening, etc.). For example, alternative models of IMAC-mediated RIRR have been proposed (31). Nevertheless, our conclusions are not likely to be strictly model-dependent, as the dynamical behaviors observed here are generic properties of excitable and oscillatory media. Although the model can be improved as more detailed physiological information becomes available, it may be useful, even in its present form, for generating predictions that can be tested experimentally. For example, following upon the observation that rotenone suppressed the ROS burst upon MPTP opening (13), we would expect rotenone to delay irreversible MPTP-mediated Ψ_M depolarization. Another prediction arising from Fig. 5 is that under conditions in which fast IMAC-mediated RIRR waves precede slow MPTP-mediated RIRR waves, such as we previously reported in isolated myocytes exposed to anoxia-reoxygenation (7), mitochondrial Ψ_M should already be partially depolarized by open IMAC channels (in the range of −40 mV) before the onset of the slow wave in which Ψ_M becomes fully depolarized due to MPTP opening. It may be possible to adjust the concentrations of Ψ_M indicators such as tetramethylrhodamine methyl ester concentrations to detect these predicted differences.

APPENDIX

The single mitochondrion model

The differential equations

The differential equations for the single mitochondrion model shown in Fig. 1 *A* are as follows:

Matrix

$$\begin{aligned}\frac{dSO_M}{dt} &= V_s - V_{SOD,M} - V_{IMAC}\\ \frac{dPO_M}{dt} &= V_{SOD,M} - V_{RED} - V_{PO,EX,M}\,,\\ \frac{dRED}{dt} &= V_{OX} - V_{RED}\end{aligned} \tag{1}$$

Intermembrane space

$$\begin{aligned}\frac{dSO_I}{dt} &= V_{IMAC}/R_{I,M} - V_{SOD,I} - V_{SO,EX,C}/R_{I,C}\\ \frac{dPO_I}{dt} &= V_{SOD,I} - V_{D,I} + V_{PO,EX,M}/R_{I,M} - V_{PO,EX,C}/R_{I,C}\end{aligned}\,, \tag{2}$$

Cytoplasm

$$\begin{aligned}\frac{dSO_C}{dt} &= V_{SO,EX,C} - V_{SOD,C}\\ \frac{dPO_C}{dt} &= V_{SOD,C} - V_{D,C} + V_{PO,EX,C}\end{aligned}, \quad (3)$$

where SO is the superoxide (O^-_2) concentration, PO the peroxide (H_2O_2) concentration, and RED the concentration of the reduced species. Subscripts M, I, and C represent matrix, intermembrane space, and cytoplasm. $R_{I,M}$ is the intermembrane space to matrix volume ratio and $R_{I,C}$ the intermembrane space/cytoplasm volume ratio. The volume ratios $R_{I,M} = 1/12$ and $R_{I,C} = 1/3$ were adopted from van Beek (32). The rate constants in Eqs. 1–3 are defined in Fig. 1 *A* and described in detail in the following sections.

O^-_2 production

Here we assume that the O^-_2 production rate V_S depends on the external ROS stress (k_{shunt}) and is accelerated by MPTP opening, i.e., $V_S = k_{shunt}(1 + \alpha_{MPTP})$, where $\alpha_{MPTP} = aP_{MPTP}$. The value a is a constant and P_{MPTP} is the MPTP open probability. According to Cortassa et al. (their Eq. 26 and Fig. A5) (15), the normal respiration rate is in the range of 0–10 mM/s. Because 1–2% of the daily oxygen consumption was estimated to mitochondrial O^-_2 production (33), a normal O^-_2 production rate of 0.05 mM/s, i.e., $k_{shunt} = 0.05$ mM/s, is reasonable. During laser scanning, we assume that the O^-_2 generation rate increases to ~10% of oxygen consumption, and therefore choose k_{shunt} to be between 0 and 0.35 mM/s. This is the same k_{shunt} range was used by Cortassa et al. (12) We assume that the MPTP opening is directly regulated by matrix H_2O_2 (because the exact ROS species derived from H_2O_2 is unknown). As there is no experimental data on exactly how MPTP opening is regulated, we set its open probability to be a Hill function of the matrix peroxide, i.e.,

$$P_{MPTP} = \frac{(PO_M)^{h_{MPTP}}}{(PO_M)^{h_{MPTP}} + (K_{PO,MPTP})^{h_{MPTP}}},$$

where h_{MPTP} is the Hill coefficient and $K_{PO,MPT}$ is the peroxide concentration at the half MPTP conductance.

O^-_2 release through IMAC

Cortassa et al. (12) formulated the IMAC channel conductance as a complex function of Ψ_M, based on experimental measurements from a 108-pS channel described by Borecký et al. (34). However, in the measurements of Borecký et al., the conductance of the channel is almost constant at the negative potentials and thus the current through the channel is $\propto \Psi_M$. As the mitochondrial potential Ψ_M is always negative, we use the simple formulation of the current-voltage relationship as

$$V_{\Psi,IMAC} = k_{\Psi,IMAC} \times P_{IMAC} \times \Psi_M,$$

where $k_{\Psi,IMAC}$ is maximum channel conductance and P_{IMAC} is the open probability of IMAC. Following the hypothesis of Cortassa et al. (12) that the opening of the IMAC is induced by O^-_2 in the intermembrane space, we assume that the open probability of IMAC follows a Hill function of intermembrane O^-_2 concentration (a Michaelis-Menten formulation was used by Cortassa et al. (12)), i.e.,

$$P_{IMAC} = 0.01 + 0.99\frac{(SO_I)^{h_{IMAC}}}{(SO_I)^{h_{IMAC}} + (K_{SO,IMAC})^{h_{IMAC}}},$$

where h_{IMAC} is the Hill coefficient, and $K_{SO,IMAC}$ is the intermembrane superoxide concentration at the half-IMAC open probability. In addition, when Ψ_M suddenly dissipates (e.g., to almost zero in the model of Cortassa et al.) once the IMAC channel opens, and then repolarizes once the IMAC channel closes, the effects of Ψ_M on O^-_2 release through the IMAC are negligible. Thus, we assume that the superoxide release rate is proportional to the superoxide in the matrix, i.e.,

$$V_{IMAC} = k_{IMAC} \times P_{IMAC} \times SO_M,$$

where k_{IMAC} is the maximum subconductance of O^-_2. Although our formulations are simpler than the formulations of Cortassa et al., when we substituted ours by those of Cortassa et al., we obtained similar bifurcation diagrams to the diagrams shown in Fig. 2, i.e., as k_{shunt} increased, we first observed the oscillatory dynamics due to the IMAC opening and then the bistable dynamics due to the MPTP opening.

O^-_2 dismutation

The dismutase rates ($V_{SOD,M}$, $V_{SOD,I}$, and $V_{SOD,C}$) are assumed to be Hill functions of O^-_2, as they are catalyzed by the superoxide dismutase species (SOD), i.e.,

$$V_{SOD,M} = k_{SOD,M}\frac{SO_M}{SO_M + K_{SOM}},$$

$$V_{SOD,I} = k_{SOD,I}\frac{SO_C}{SO_C + K_{SOI}},$$

and

$$V_{SOD,C} = k_{SOD,C}\frac{SO_C}{SO_C + K_{SOC}},$$

where $k_{SOD,I}$, $k_{SOD,C}$, and $k_{SOD,M}$ are maximum dismutation rates, and K_{SOM}, K_{SOI}, and K_{SOC} are the Michaelis-Menten constants. Because SOD inside the matrix may differ from outside, we assume that K_{SOI} and K_{SOC} are the same, but different from K_{SOM}. The maximum SOD production rates in the intermembrane space ($k_{SOD,I}$) and cytoplasm ($k_{SOD,C}$) are set at 0.1 mM/s, which are in the same range used by Cortassa et al. (their Fig. A4) (12). We used a smaller value for the matrix SOD rate, i.e., $k_{SOD,M} = 0.01$ mM/s.

H_2O_2 degradation

The matrix H_2O_2 degradation rate is proportional to the matrix H_2O_2 concentration (PO_M), and is also regulated by the ratio of reduced/oxidized species,

$$REDOX = \frac{RED}{OX},$$

where

$$OX = RED_{Total} - RED,$$

and where RED_{Total} is the total reduced and oxidized species concentration which is set to be 3 mM according to Aon et al. (25). The OX can be converted back to RED with a rate

$$V_{OX} = k_{OX}OX = k_{OX}(RED_{Total} - RED),$$

and k_{OX} is a constant. The H_2O_2 degradation rate is set as

$$V_{RED} = k_{RED}\frac{REDOX}{REDOX + K_{REDOX}}PO_M,$$

where k_{RED} is constant and K_{REDOX} is the Michaelis-Menten constant. H_2O_2 in the cytoplasm (PO_C) and in the intermembrane space (PO_I) are assumed to be degraded with fixed rates, i.e.,

$$V_{D,I} = k_{D,I}PO_I$$

and

$$V_{D,C} = k_{D,C} PO_C,$$

where $k_{D,I}$ and $k_{D,C}$ are constants.

O^-_2 and H_2O_2 diffusion

O^-_2 diffuses freely between the intermembrane space and cytoplasm, so we simply set the diffusion rate as

$$V_{SO,EX,C} = k_{SO,EX,C}(SO_I - SO_C),$$

where $k_{SO,EX,C}$ is a constant. H_2O_2 diffuses freely between different compartments and we set the diffusion rates as

$$V_{PO,EX,C} = k_{PO,EX,C}(PO_I - PO_C)$$

and

$$V_{PO,EX,M} = k_{PO,EX,M}(PO_M - PO_I),$$

where $k_{PO,EX,M}$ and $k_{PO,EX,C}$ are constants. Because the mitochondrial intermembrane space is close to the matrix, we assume that the exchange between intermembrane space and matrix is much faster than the exchange between intermembrane space and cytoplasm, i.e., $k_{SO,EX,M} = 10k_{SO,EX,C}$. Based on our own measurements (P. Korge and J. N. Weiss, unpublished data), we obtained an oxygen diffusion coefficient in water to be ~1400 $\mu m^2/s$. The diffusion coefficient of oxygen in blood was estimated to be 1200 $\mu m^2/s$ (35,36). In this study, we set the diffusion coefficients of O^-_2 and H_2O_2 to be $D = 112.5\ \mu m^2/s$, assuming that the complex cytoplasm environment causes a much slower diffusion. Using this diffusion rate, the rate constant is estimated as $k_{SO,EX,C} = 4D/\Delta x^2 = 5000\ s^{-1}$.

The spatial mitochondrial network model

The single mitochondrion model is used for each unit. The differential equations for the matrix in unit are

$$\begin{aligned}
\frac{dSO_M}{dt} &= V_s - V_{SOD,M} - V_{IMAC} \\
\frac{dPO_M}{dt} &= V_{SOD,M} - V_{RED} - V_{PO,EX,M} \\
\frac{dRED}{dt} &= V_{OX} - V_{RED} \\
\frac{d\Psi_M}{dt} &= V_{\Psi,S} - V_{\Psi,U} - V_{\Psi,IMAC} - V_{\Psi,MPTP}.
\end{aligned} \tag{4}$$

We add the mitochondrial membrane potential (Ψ_M) into the system, as described by the fourth expression in Eq.4. In this model, we simply use the Ψ_M production rate as $V_{\Psi,S} = 3.5$ V/s, and assume Ψ_M usage (including leak) rate to be $V_{\Psi,U} = k_{\Psi,U}\Psi_M$. The current-voltage relationship of IMAC is (see O^-_2 Release Through IMAC):

$$V_{\Psi,IMAC} = k_{\Psi,IMAC}\left[0.01 + 0.99\frac{(SO_I)^{p_{IAMC}}}{(SO_I)^{p_{IMAC}} + (K_{SO,IMAC})^{p_{IAMC}}}\right]\Psi_M.$$

We also assume that MPTP conductance is proportional to its opening probability, and thus the current-voltage relationship is

$$V_{\Psi,MPTP} = k_{\Psi,MPTP}\frac{(PO_M)^{p_{MPTP}}}{(PO_M)^{p_{MPTP}} + (K_{PO,MPTP})^{p_{MPTP}}}\Psi_M.$$

TABLE 1 Model parameters

Symbols	Description	Value	Unit
k_{shunt}	O^-_2 production rate constant.	0–0.35	mM/s
$K_{PO,MPTP}$	H_2O_2 concentration at the half MPTP conductance.	0.015	mM
h_{MPTP}	Hill coefficient of MPTP activation kinetics.	10	
$k_{SOD,M}$	Maximum matrix SOD rate.	0.01	mM/s
$k_{SOD,I}$	Maximum SOD rate constant in the intermembrane space.	0.1	mM/s
$k_{SOD,C}$	Maximum SOD rate constant in the cytoplasm.	0.1	mM/s
K_{SOM}	Michaelis-Menten constant of matrix SOD.	0.02	mM
K_{SOI}	Michaelis-Menten constant of intermembrane space SOD.	0.02	mM
K_{SOC}	Michaelis-Menten constant of cytoplasmic SOD.	0.02	mM
RED_{Total}	Total concentration of reduced/oxidized species in the matrix.	3	mM
k_{RED}	Rate constant of H_2O_2 degradation in the matrix.	10,000	s^{-1}
K_{REDOX}	Michaelis-Menten constant of H_2O_2 degradation in the matrix.	50	
$k_{D,I}$	H_2O_2 degradation rate constant in the intermembrane space.	0.05	s^{-1}
$k_{D,C}$	H_2O_2 degradation rate constant in the cytoplasm.	0.05	s^{-1}
k_{IMAC}	Maximum IMAC O^-_2 conductance.	0.5	s^{-1}
h_{IMAC}	Hill coefficient of IMAC activation kinetics.	3	
$K_{SO,IMAC}$	O^-_2 concentration at the half-IMAC conductance.	0.004	mM
$k_{SO,EX,C}$	O^-_2 diffusion rate between intermembrane space and cytoplasm.	5000	s^{-1}
$K_{PO,EX,M}$	H_2O_2 diffusion rate between matrix and intermembrane space.	50,000	s^{-1}
$K_{PO,EX,C}$	H_2O_2 diffusion rate between intermembrane space and cytoplasm.	5000	s^{-1}
k_{OX}	Rate constant of oxidized species to reduced species.	0.08	s^{-1}
$R_{I,C}$	Intermembrane space to cytoplasm volume ratio.	1/12	
$R_{I,M}$	Intermembrane space/matrix volume ratio.	1/3	
a	O^-_2 production rate constant induced by MPTP.	0.5	
$k_{\Psi,U}$	Constant of membrane potential usage.	19.2	s^{-1}
$k_{\Psi,IMAC}$	Constant of membrane potential loss due to IMAC opening.	50	s^{-1}
$k_{\Psi,MPTP}$	Constant of membrane potential loss due to MPTP opening.	100	s^{-1}
D	Diffusion constant.	112.5	$\mu m^2/s$

The differential equations for O^-_2 and H_2O_2 in the intermembrane space (for any voxel in Fig. 1 *B*) are

$$\begin{aligned}\frac{dSO_\mathrm{I}}{dt} &= V_\mathrm{IMAC}/R_\mathrm{I,M} - V_\mathrm{SOD,I} + \Delta SO/\alpha \\ \frac{dPO_\mathrm{I}}{dt} &= V_\mathrm{SOD,I} + V_\mathrm{PO,EX,M}/R_\mathrm{I,M} - V_\mathrm{D,I} + \Delta PO/\alpha,\end{aligned} \tag{5}$$

where

$$\Delta SO = k\left(\sum_{\mathrm{k}=1}^{4} SO_\mathrm{k} - 4SO_\mathrm{I}\right)$$

and

$$\Delta PO = k\left(\sum_{\mathrm{k}=1}^{4} PO_\mathrm{k} - 4PO_\mathrm{I}\right)$$

are the fluxes between the intermembrane voxel and its four neighboring cytoplasmic voxels (see Fig. 1 *C*). The values $k = D/\Delta x^2$ and $D = 112.5\ \mu\mathrm{m}^2/\mathrm{s}$ constitute the diffusion constant and $\Delta x = 0.3\ \mu\mathrm{m}$. The value $\alpha = 2/3$ is the volume ratio of the intermembrane voxel and the cytoplasmic voxel.

We assume that O^-_2 and H_2O_2 diffuse freely in the cytoplasmic space. The governing equations are

$$\begin{aligned}\frac{\partial SO}{\partial t} &= -V_\mathrm{SOD,C} + D\left(\frac{\partial^2}{\partial x^2} + \frac{\partial^2}{\partial y^2}\right)SO \\ \frac{\partial PO}{\partial t} &= V_\mathrm{SOD,C} - V_\mathrm{D,C} + D\left(\frac{\partial^2}{\partial x^2} + \frac{\partial^2}{\partial y^2}\right)PO.\end{aligned} \tag{6}$$

At the border between intermembrane space and cytoplasm (the border between the *shaded voxel* and the *open voxel* in Fig. 1 *C*), the boundary condition is

$$\begin{aligned}\left.\frac{\partial SO}{\partial x}\right|_\mathrm{IC} &= -\Delta SO_\mathrm{k} \\ \left.\frac{\partial PO}{\partial x}\right|_\mathrm{IC} &= -\Delta PO_\mathrm{k},\end{aligned}$$

where

$$\Delta SO_\mathrm{k} = k(SO_\mathrm{k} - SO_\mathrm{I}) \text{ and } \Delta PO_\mathrm{k} = k(PO_\mathrm{k} - SO_\mathrm{I}).$$

We use no-flux boundary condition for the whole domain, i.e.,

$$\left.\frac{\partial SO}{\partial x}\right|_{0,L_\mathrm{x}} = \left.\frac{\partial PO}{\partial x}\right|_{0,L_\mathrm{x}} = \left.\frac{\partial SO}{\partial y}\right|_{0,L_\mathrm{y}} = \left.\frac{\partial PO}{\partial y}\right|_{0,L_\mathrm{y}} = 0,$$

where L_x and L_y are the dimensions of the two-dimensional network.

Except for the parameters defined above, other parameters were arbitrarily adjusted to produce the dynamics in the model. All parameters are listed in Table 1.

This study was supported by National Institutes of Health grant Nos. P01 HL080111 and R01 HL095663, National Science Foundation of China, (grant No. 10971152 to L.Y.), and by the Laubisch and Kawata endowments.

We thank Henry Honda and Jun-Hai Yang for helpful discussions.

REFERENCES

1. Stanley, W. C., F. A. Recchia, and G. D. Lopaschuk. 2005. Myocardial substrate metabolism in the normal and failing heart. *Physiol. Rev.* 85:1093–1129.
2. Saks, V., P. Dzeja, …, T. Wallimann. 2006. Cardiac system bioenergetics: metabolic basis of the Frank-Starling law. *J. Physiol.* 571:253–273.
3. Hüser, J., and L. A. Blatter. 1999. Fluctuations in mitochondrial membrane potential caused by repetitive gating of the permeability transition pore. *Biochem. J.* 343:311–317.
4. Aon, M. A., S. Cortassa, …, B. O'Rourke. 2003. Synchronized whole cell oscillations in mitochondrial metabolism triggered by a local release of reactive oxygen species in cardiac myocytes. *J. Biol. Chem.* 278:44735–44744.
5. Aon, M. A., S. Cortassa, and B. O'Rourke. 2004. Percolation and criticality in a mitochondrial network. *Proc. Natl. Acad. Sci. USA.* 101:4447–4452.
6. Brady, N. R., S. P. Elmore, …, H. V. Westerhoff. 2004. Coordinated behavior of mitochondria in both space and time: a reactive oxygen species-activated wave of mitochondrial depolarization. *Biophys. J.* 87:2022–2034.
7. Honda, H. M., P. Korge, and J. N. Weiss. 2005. Mitochondria and ischemia/reperfusion injury. *Ann. N. Y. Acad. Sci.* 1047:248–258.
8. Aon, M. A., S. Cortassa, …, B. O'Rourke. 2006. Mitochondrial criticality: a new concept at the turning point of life or death. *Biochim. Biophys. Acta.* 1762:232–240.
9. Aon, M. A., S. Cortassa, and B. O'Rourke. 2006. The fundamental organization of cardiac mitochondria as a network of coupled oscillators. *Biophys. J.* 91:4317–4327.
10. Weiss, J. N., L. Yang, and Z. Qu. 2006. Systems biology approaches to metabolic and cardiovascular disorders: network perspectives of cardiovascular metabolism. *J. Lipid Res.* 47:2355–2366.
11. Brady, N. R., A. Hamacher-Brady, …, R. A. Gottlieb. 2006. A wave of reactive oxygen species (ROS)-induced ROS release in a sea of excitable mitochondria. *Antioxid. Redox Signal.* 8:1651–1665.
12. Cortassa, S., M. A. Aon, …, B. O'Rourke. 2004. A mitochondrial oscillator dependent on reactive oxygen species. *Biophys. J.* 87:2060–2073.
13. Zorov, D. B., C. R. Filburn, …, S. J. Sollott. 2000. Reactive oxygen species (ROS)-induced ROS release: a new phenomenon accompanying induction of the mitochondrial permeability transition in cardiac myocytes. *J. Exp. Med.* 192:1001–1014.
14. Zorov, D. B., M. Juhaszova, and S. J. Sollott. 2006. Mitochondrial ROS-induced ROS release: an update and review. *Biochim. Biophys. Acta.* 1757:509–517.
15. Cortassa, S., M. A. Aon, …, B. O'Rourke. 2003. An integrated model of cardiac mitochondrial energy metabolism and calcium dynamics. *Biophys. J.* 84:2734–2755.
16. Turrens, J. F., A. Alexandre, and A. L. Lehninger. 1985. Ubisemiquinone is the electron donor for superoxide formation by complex III of heart mitochondria. *Arch. Biochem. Biophys.* 237:408–414.
17. Messner, K. R., and J. A. Imlay. 2002. Mechanism of superoxide and hydrogen peroxide formation by fumarate reductase, succinate dehydrogenase, and aspartate oxidase. *J. Biol. Chem.* 277:42563–42571.
18. Yankovskaya, V., R. Horsefield, …, S. Iwata. 2003. Architecture of succinate dehydrogenase and reactive oxygen species generation. *Science.* 299:700–704.
19. Turrens, J. F. 2003. Mitochondrial formation of reactive oxygen species. *J. Physiol.* 552:335–344.
20. Batandier, C., X. Leverve, and E. Fontaine. 2004. Opening of the mitochondrial permeability transition pore induces reactive oxygen species production at the level of the respiratory chain complex I. *J. Biol. Chem.* 279:17197–17204.
21. Wang, W., H. Fang, …, H. Cheng. 2008. Superoxide flashes in single mitochondria. *Cell.* 134:279–290.
22. Bers, D. M. 2001. Excitation-Contraction Coupling and Cardiac Contractile Force. Kluwer Academic, Dordrecht, The Netherlands.
23. Chen, Q., S. Moghaddas, …, E. J. Lesnefsky. 2008. Ischemic defects in the electron transport chain increase the production of reactive oxygen species from isolated rat heart mitochondria. *Am. J. Physiol. Cell Physiol.* 294:C460–C466.

24. Tyson, J. J., K. C. Chen, and B. Novak. 2003. Sniffers, buzzers, toggles and blinkers: dynamics of regulatory and signaling pathways in the cell. *Curr. Opin. Cell Biol.* 15:221–231.

25. Aon, M. A., S. Cortassa, …, B. O'Rourke. 2007. Sequential opening of mitochondrial ion channels as a function of glutathione redox thiol status. *J. Biol. Chem.* 282:21889–21900.

26. Wu, F., F. Yang, …, D. A. Beard. 2007. Computer modeling of mitochondrial tricarboxylic acid cycle, oxidative phosphorylation, metabolite transport, and electrophysiology. *J. Biol. Chem.* 282:24525–24537.

27. Dash, R. K., and D. A. Beard. 2008. Analysis of cardiac mitochondrial Na^{+}-Ca^{2+} exchanger kinetics with a biophysical model of mitochondrial Ca^{2+} handling suggests a 3:1 stoichiometry. *J. Physiol.* 586: 3267–3285.

28. Yang, J. H., L. Yang, …, J. N. Weiss. 2008. Glycolytic oscillations in isolated rabbit ventricular myocytes. *J. Biol. Chem.* 283:36321–36327.

29. Zhou, L., J. E. Salem, …, M. E. Cabrera. 2005. Mechanistic model of cardiac energy metabolism predicts localization of glycolysis to cytosolic subdomain during ischemia. *Am. J. Physiol. Heart Circ. Physiol.* 288:H2400–H2411.

30. Zhou, L., M. E. Cabrera, …, W. C. Stanley. 2006. Regulation of myocardial substrate metabolism during increased energy expenditure: insights from computational studies. *Am. J. Physiol. Heart Circ. Physiol.* 291:H1036–H1046.

31. Saleet Jafri, M., and M. Kotulska. 2006. Modeling the mechanism of metabolic oscillations in ischemic cardiac myocytes. *J. Theor. Biol.* 242:801–817.

32. van Beek, J. H. G. M. 2007. Adenine nucleotide-creatine-phosphate module in myocardial metabolic system explains fast phase of dynamic regulation of oxidative phosphorylation. *Am. J. Physiol. Cell Physiol.* 293:C815–C829.

33. Cadenas, E., and K. J. Davies. 2000. Mitochondrial free radical generation, oxidative stress, and aging. *Free Radic. Biol. Med.* 29:222–230.

34. Borecký, J., P. Jezek, and D. Siemen. 1997. 108-pS channel in brown fat mitochondria might be identical to the inner membrane anion channel. *J. Biol. Chem.* 272:19282–19289.

35. Wyman, J. 1966. Facilitated diffusion and the possible role of myoglobin as a transport mechanism. *J. Biol. Chem.* 241:115–121.

36. Keener, J. P., and J. Sneyd. 1998. Mathematical Physiology. Springer, New York.